

# Analyst

Accepted Manuscript



This is an *Accepted Manuscript*, which has been through the Royal Society of Chemistry peer review process and has been accepted for publication.

*Accepted Manuscripts* are published online shortly after acceptance, before technical editing, formatting and proof reading. Using this free service, authors can make their results available to the community, in citable form, before we publish the edited article. We will replace this *Accepted Manuscript* with the edited and formatted *Advance Article* as soon as it is available.

You can find more information about *Accepted Manuscripts* in the [Information for Authors](#).

Please note that technical editing may introduce minor changes to the text and/or graphics, which may alter content. The journal's standard [Terms & Conditions](#) and the [Ethical guidelines](#) still apply. In no event shall the Royal Society of Chemistry be held responsible for any errors or omissions in this *Accepted Manuscript* or any consequences arising from the use of any information it contains.

## ARTICLE

# Label-free phenotyping of peripheral blood lymphocytes by infrared imaging

Cite this: DOI:  
10.1039/x0xx00000x

M. Verdonck,<sup>a</sup> S. Garaud,<sup>b</sup> H. Duvillier,<sup>c</sup> K. Willard-Gallo<sup>b</sup> and E. Goormaghtigh<sup>a</sup>

Received 00th Xxxxxx XXXX,  
Accepted 00th Xxxxxx XXXX

DOI: 10.1039/x0xx00000x

www.rsc.org/

It is now widely accepted that the immune microenvironment of tumors and more precisely Tumor Infiltrating Lymphocytes (TIL) play an important role in cancer development and outcome. TILs are considered to be important prognostic and predictive factors based on a growing body of clinical evidence; however, their presence at the tumor site is not currently assessed routinely. FTIR (Fourier Transform Infrared) imaging has proven it has value in studying a range of tumors, particularly for characterizing tumor cells. Currently, very little is known about the potential for FTIR imaging to characterize TIL. The present proof of concept study investigates the ability of FTIR imaging to identify the principal lymphocyte subpopulations present in human peripheral blood (PB). A negative cell isolation method was employed to select pure, label-free, helper T cells (CD4<sup>+</sup>), cytotoxic T cells (CD8<sup>+</sup>) and B cells (CD19<sup>+</sup>) from six healthy donors PB by Fluorescence Activated Cell Sorting (FACS). Cells were centrifuged onto Barium Fluoride windows and ten infrared images were recorded for each lymphocyte subpopulation from all six donors. After spectral pre-treatment, statistical analyses were performed. Unsupervised Principal Component Analyses (PCA) revealed that in the absence of donor variability, CD4<sup>+</sup> T cells, CD8<sup>+</sup> T cells and B cells each display distinct IR spectral features. Supervised Partial Least Square Discriminant Analyses (PLS-DA) demonstrated that the differences between the three lymphocyte subpopulations are reflected in their IR spectra, permitting their individual identification even when significant donor variability is present. Our results also show that a distinct spectral signature is associated with antibody binding. To our knowledge this is the first study reporting that FTIR imaging can effectively identify T and B lymphocytes and differentiate helper T cells from cytotoxic T cells. This proof of concept study demonstrates that FTIR imaging is a reliable tool for the identification of lymphocyte subpopulations and has the potential for use in characterizing TIL.

## Introduction

Over the past few decades, Fourier Transform Infrared spectroscopy has been shown to be a useful tool for obtaining unique fingerprints of different cell types. FTIR is receptive to all molecules (proteins, lipids, sugars, etc.) present in cells, and importantly, is also sensitive to protein conformation<sup>1-5</sup> as well as to the nature, chain length and unsaturation level of lipids.<sup>6,7</sup> In turn, cell line spectra reflect differences in cell cycle,<sup>8-14</sup> confluence,<sup>15</sup> cell strain<sup>16</sup> and interestingly the various metabolic perturbations induced by potent anticancer drugs, thus recognizing some level of 'mode of action' for a given drug.<sup>17-22</sup> When coupled to a microscope, this technique provides spatially resolved information on the chemical composition of the different cell types present in tissue sections, and as such is recognized as an emerging tool for histopathological analyses.<sup>23-26</sup> Because of its potential to probe chemical constituents without dyes or specific reagents, FTIR imaging has the potential to become a powerful tool in cancer diagnosis as a complement to existing methods.<sup>23</sup> In the research setting, infrared spectroscopy has already proven to be

valuable for studying many cancers, including cervix,<sup>27</sup> breast,<sup>28-31</sup> prostate,<sup>32-35</sup> lung,<sup>36,37</sup> colon,<sup>38-41</sup> skin,<sup>42</sup> liver,<sup>43</sup> oesophagus<sup>44</sup> and brain.<sup>45</sup>

The presence of infiltrating immune cells in some solid tumor types is now considered as a new and important prognostic and predictive marker.<sup>46-50</sup> Immune cells are thought to play a dual role during tumor development, by promoting tumor growth and invasiveness and/or mediating tumor cell killing, depending on the lymphocyte subpopulations present at the tumor site.<sup>47,49,51,52</sup> Due to costly and time-consuming aspects of current IHC or IF staining methods for lymphocyte characterization their presence at the tumor site remains underinvestigated and is only beginning to be used in the clinical decision-making process for some tumor types, such as breast cancer.<sup>50</sup> FTIR imaging can potentially be employed to identify individual lymphocyte subpopulations on a single microscope slide without using specific antibodies. FTIR imaging has been shown to produce valuable information on tumor cells; however, very little is known about its usefulness for investigating tumor infiltrating lymphocytes.

Presently, very few articles on infrared spectroscopic studies of lymphocytes have been published. The first study conducted by Schultz et al. in 1996 revealed that chronic lymphocytic leukemia could be studied using FTIR spectroscopy.<sup>53</sup> They used this vibrational technique to not only detect differences between normal and abnormal cells but also detect differences of drug resistance by malignant subclones.<sup>54</sup> The usefulness of FTIR microscopy was further demonstrated for follow-up assessments in childhood leukemia<sup>55</sup> and studying radiation-induced apoptosis in human lymphocytes.<sup>56</sup> Recently, FTIR imaging has been shown to be an interesting tool for detecting lymphocyte activation.<sup>57,58</sup> To our knowledge, only one study suggests the potential for using FTIR imaging to identify and distinguish B and T cells.<sup>59</sup> In 2005, Krafft et al. used positive cell selection to discriminate CD19<sup>+</sup> B cells from CD3<sup>+</sup> T cells (a pan T cell marker) without differentiating the major T cell subpopulations (CD4<sup>+</sup> helper and CD8<sup>+</sup> cytotoxic T cells).

The work presented in this study addresses lymphocyte subpopulation identification using CD4<sup>+</sup>, CD8<sup>+</sup> and CD19<sup>+</sup> cells purified from the PB of Healthy Donors (HD). To avoid artefacts related with an antibody presence, we designed a negative purification scheme where each lymphocyte subpopulation was isolated without specific antibody binding to the target population.

## Materials and Methods

### Isolation of peripheral blood mononuclear cells from healthy donors

For each of the six HD, eight to ten PB samples (80 to 100 ml) were collected in heparin tubes. The collected blood was then immediately diluted with an equal volume of RPMI 1640 (Lonza, Verviers, Belgium). The diluted blood (30 ml) was layered over 15 ml of Lymphoprep<sup>TM</sup> (Axis-Shield, Oslo, Norway) in a 50 ml centrifuge tube and centrifuged at 1800 rpm for 30 minutes. The Peripheral Blood Mononuclear Cells (PBMC) were harvested from the sample/medium interface where they formed a distinct band. The PBMC fraction was diluted by adding RPMI 1640 and the cells were pelleted by centrifugation for 10 minutes at 300 x g. The PBMC were washed an additional three times with RPMI 1640 and then counted using a Z2 Coulter Counter cell counter (Beckman Coulter, California, USA). The PBMC were held at 4°C prior to antibody labelling.

### CD4<sup>+</sup>, CD8<sup>+</sup> and CD19<sup>+</sup> cell sorting

The three major lymphocyte subpopulations found in PB (CD4, CD8 and CD19 positive cells) were isolated from total PBMCs using Fluorescence Activated Cell Sorting (FACS) and a negative staining protocol as described in Results. To separately isolate the three unlabelled lymphocyte subpopulations, different combinations of fluorophore-conjugated antibodies were added to aliquots of the PBMCs. The antibodies used included FITC-conjugated anti-CD4 (ref. 130-080-501, Miltenyi Biotec, Bergisch Gladbach, Germany), APC-conjugated anti-CD19 (ref. 555415, BD Biosciences, New Jersey, USA), ECD-conjugated anti-CD3, FITC-conjugated anti-CD8 and PE-conjugated anti-CD56 (refs. A07748, A07756 and A07788, Beckman Coulter, California, USA). PBMC were labelled with the specified antibodies for 1 hour at 4°C. The volume of antibody was calculated to ensure a saturating concentration for 10<sup>6</sup> cells. The unlabelled lymphocytes were sorted on a MoFlo Astrios (Beckman

Coulter, California, USA). The purity of the sorted CD4<sup>+</sup>, CD8<sup>+</sup> and CD19<sup>+</sup> cells was determined by positive antibody labelling a small fraction of the purified cells for evaluating their purity on a Navios cytometer (Beckman Coulter, California, USA). Flow cytometry data were analysed using the Kaluza software (Beckman Coulter, California, USA). For infrared spectral recording, cells were centrifuged onto a Barium Fluoride window of 40x26x2 mm<sup>3</sup> (ACM, Villiers Saint Frédéric, France) using a Shandon CytoSpin centrifuge and subsequently air-dried.

### FTIR measurements

The IR data were collected using a Hyperion 3000 IR imaging system (Bruker Optics, Ettlingen, Germany), equipped with a liquid nitrogen cooled 64 x 64 Mercury Cadmium Telluride (MCT) Focal Plane Array (FPA) detector. The data were collected in transmission mode. The size of an image covered an area of 180 x 180 μm<sup>2</sup> composed of 4096 pixels of 2.8 x 2.8 μm<sup>2</sup>. Each pixel corresponds to an IR spectrum. To record 256 scans of each pixel at a spectral resolution of 8 cm<sup>-1</sup> took approximately 5 min. It should be noted that spatial resolution is significantly lower than the pixel size. For each lymphocyte subpopulation isolated from every donor, ten IR images were recorded. Spectra were therefore acquired on several thousands of cells.

### Data analysis

#### Pre-processing of infrared spectra

All spectra were preprocessed as follows: water vapor contribution was subtracted as previously described<sup>60,61</sup> with 1956-1935 cm<sup>-1</sup> as reference peak and the CO<sub>2</sub> peak flattened between 2450 and 2250 cm<sup>-1</sup>. The spectra were baseline-corrected. Straight lines were interpolated between the spectra points at 3620, 2995, 2800, 2395, 2247, 1765, 1724, 1480, 1355, 1144 and 950 cm<sup>-1</sup> and subtracted from each spectrum. Spectra were normalized for equal area between 1725 and 1481 cm<sup>-1</sup> (Amide I and II peaks). The Signal to Noise ratio (S/N) was then checked on each spectrum. It was required to be higher than 300 with noise defined as the standard deviation in the 2000-1900 cm<sup>-1</sup> region of the spectrum and signal defined as the maximum of the curve between 1750 and 1480 cm<sup>-1</sup> after subtracting a baseline passing through these two points. Finally, some rare spectra with normalized absorbance lower than -5 (negative lobe) and a maximum above 120 (saturation) were discarded. To avoid abrupt refractive index changes we always selected areas of the sample with contiguous cells. Visual inspection of the spectra as well as systematic screening for negative lobes on the left hand side of the Amide I band did not reveal significant dispersive artefacts. As Mie scattering corrections rely on simplified models<sup>62-66</sup> and dispersive artefacts were minor in the present work, we preferred to not apply such a correction.

#### Statistical analyses

In order to observe the intrinsic proximities and distances within the data set and to group IR spectra according to their similarity, unsupervised Principal Component Analyses (PCA) were performed. Supervised Partial Least Square Discriminant Analyses (PLS-DA) were also performed on the data set to extract latent variables that enable the construction of a factor capable of predicting a class.

Correction of the IR spectra for water vapor and CO<sub>2</sub> contributions, baseline subtraction, normalization, quality

filters, principal component analyses and partial least square discriminant analyses were carried out using Kinetics, a custom made program running under Matlab (Matlab, Mathworks Inc).

## Results

### Isolation of label free lymphocyte subpopulations from the peripheral blood of healthy donors

CD4<sup>+</sup> and CD8<sup>+</sup> T lymphocytes as well as CD19<sup>+</sup> B lymphocytes were purified from PB samples taken from HD as described in Materials and Methods and illustrated schematically in **Figure 1**. Briefly, the PBMC fraction from blood was harvested by density gradient centrifugation. Lymphocytes were then FACS sorted using a negative isolation approach to obtain lymphocytes without antibody on their surface for recording the infrared images. For each blood donor, the PBMC were divided into three fractions for the separate and successive cell sorting experiments. For each group, the unwanted lymphocyte subpopulations were labelled with a cocktail of antibodies used to positively exclude these cellular subsets by sorting them into one receptacle while the desired unlabelled lymphocyte subpopulation was sorted into another (negative cell sorting). For example, to isolate unlabelled CD4<sup>+</sup> T lymphocytes, non-CD4<sup>+</sup> cells, *i.e.* CD8<sup>+</sup> T cells, CD19<sup>+</sup> B cells and CD56<sup>+</sup> Natural Killer (NK) cells, were labelled with the cocktail of fluorophore-conjugated antibodies listed in Materials and Methods. A similar sorting strategy was repeated for isolating unlabelled CD8<sup>+</sup> and CD19<sup>+</sup> cells. The different sorting strategies and antibody combinations are shown in **Figure 1**.

Flow cytometry was used to analyse each cell population before and after sorting and assess the purity of the final sorted populations. As an example, the dot plots and histogram in **Figure 2** show the analysis of the unlabelled CD4<sup>+</sup> T cell sorting experiment from Donor 6. In this experiment, the PBMC contained 78% lymphocytes including 36% CD8<sup>+</sup> T cells, 24% CD56<sup>+</sup> NK cells and 6% B cells (see **Figure 2A**). As shown in **Figure 2B**, analysis of the remaining unlabelled cells shows they are exclusively CD8<sup>-</sup> CD56<sup>-</sup> and CD19<sup>-</sup> lymphocytes. A post-sort labelling was performed on an aliquot of the negatively harvested population to determine the CD4<sup>+</sup> T cell purity. **Figure 2C** shows the unlabelled CD4<sup>+</sup> T lymphocytes are 94% pure. The number of cells, IR spectra and purities are listed in **Table 1**, which also shows that negative cell sorting can be used to isolate cellular subpopulations with a high degree of purity, similar to that obtained with other methods such as magnetic bead isolation kits.

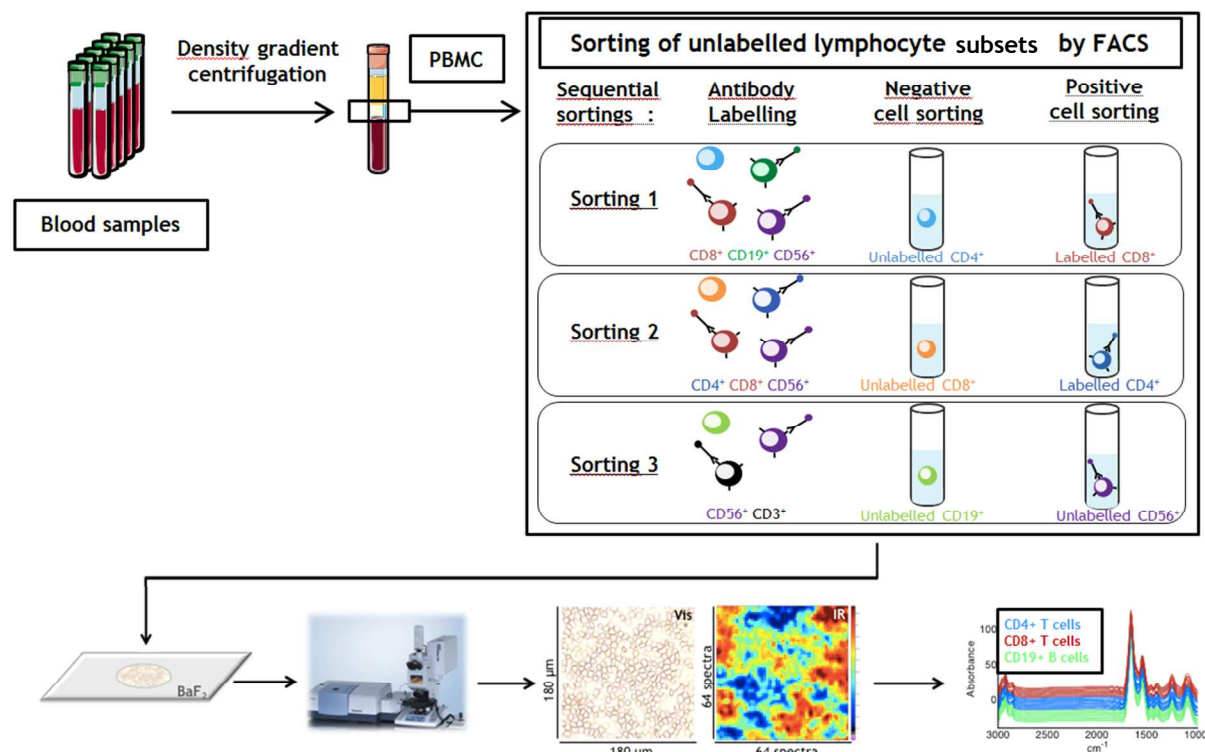


**Figure 1:** Schematic representation of the experimental workflow. For each of the six Healthy Donors, 80 to 100 ml of blood was collected by venipuncture. Isolation of PBMC was performed using density gradient centrifugation. Three sequential sortings on a flow cytometer were performed to isolate the three label-free lymphocyte subpopulations. The harvested cells were then centrifuged onto BaF<sub>2</sub> microscope slides. For each lymphocyte subpopulation ten infrared images containing 4096 spectra were acquired using a Bruker Hyperion 3000 FTIR microscope. Spectral data were then pre-processed as described in Materials and Methods.

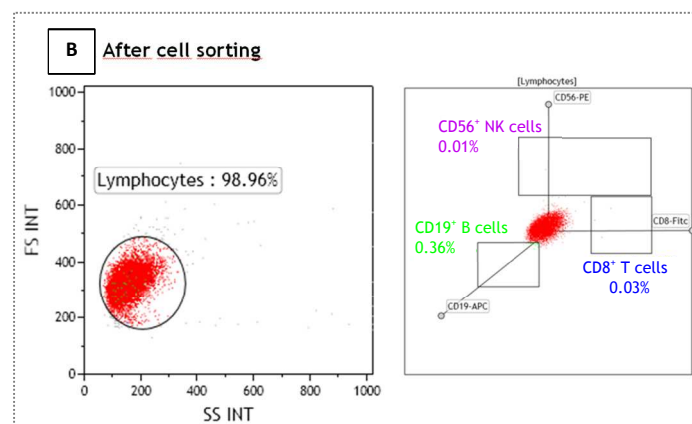
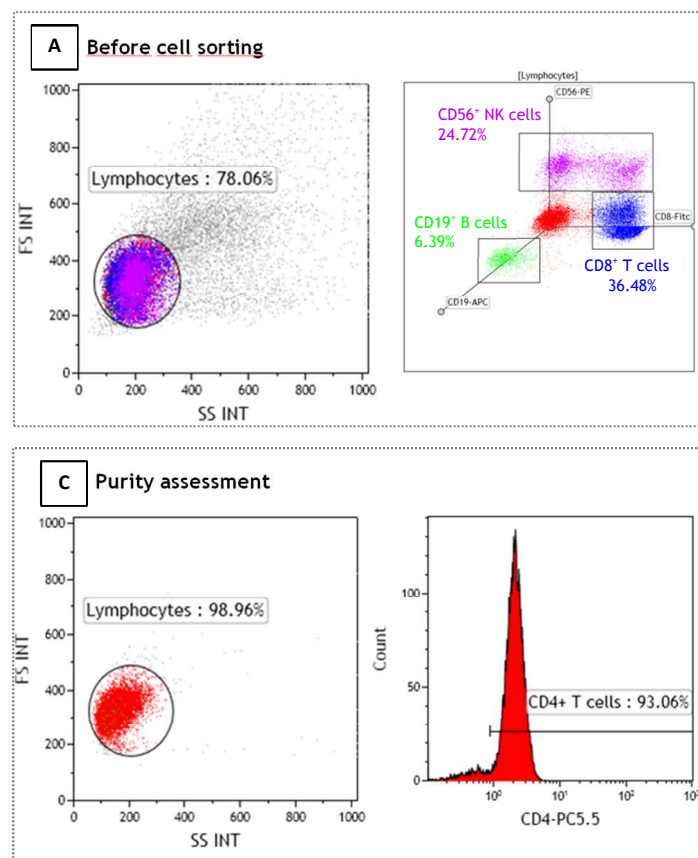


**Figure 2:** An example of flow cytometry analyses for negatively sorted  $CD4^+$  T cells from Donor 6. In the dot plots before (A) and after (B) cell sorting, each dot represents a single element (cell) passing through the flow cytometer. A gate is first used to identify the total viable lymphocyte population (left) with three subsequent gates (right) marking the non- $CD4^+$  lymphocyte subpopulations, i.e.  $CD8^+$  cytotoxic T cells,  $CD19^+$  B cells and  $CD56^+$  NK cells. A histogram depicting  $CD4$  post-sort labelling shows the purity of the unlabelled sorted cells (C).

**Table 1:** The number, purity and infrared spectra of the purified lymphocytes are shown for all six HD. In some experiments, IR spectra were not acquired either because of problems when centrifuging the cells onto the microscope slides, or poor quality of the spectra (S/N ratio too low) or low cell purity.

		CD4	CD8	CD19
Donor 1	IR spectra	✓	✓	✓
	Nb of cells	$4 \times 10^6$	$5.5 \times 10^6$	$1.5 \times 10^6$
	Purity	70%	82%	98%
Donor 2	IR spectra	✓	✓	✓
	Nb of cells	$7 \times 10^6$	$1 \times 10^6$	$2 \times 10^6$
	Purity	91%	74%	99%
Donor 3	IR spectra	✓	✓	✓
	Nb of cells	$3 \times 10^6$	$2 \times 10^6$	$1.7 \times 10^6$
	Purity	95%	88%	43%
Donor 4	IR spectra	✓	-	-
	Nb of cells	$1.8 \times 10^6$	$2 \times 10^6$	$7 \times 10^5$
	Purity	96%	88%	96%
Donor 5	IR spectra	-	-	✓
	Nb of cells	$5 \times 10^6$	$4 \times 10^6$	$1.3 \times 10^6$
	Purity	90%	80%	95%
Donor 6	IR spectra	✓	✓	-
	Nb of cells	$3 \times 10^6$	$5 \times 10^6$	$1.2 \times 10^6$
	Purity	93%	93%	97%

### Unsupervised statistical analyses

A total of approximately 200,000 purified lymphocyte IR spectra were recorded to create a spectral database. Due to this large volume of data, analyses were performed both on mean spectra and subsets randomly selected from the spectral database.

Principal Component Analyses (PCA) and unsupervised multivariate approaches were independently applied to the spectra from each donor's  $CD4^+$  T lymphocytes,  $CD8^+$  T lymphocytes and B lymphocytes. As an example, the results from Donor 1 are shown in **Figure 3**, whereas for each donor, ten IR images were recorded for each lymphocyte subpopulation. For each unit image (4096 spectra), every single spectrum was processed as described in Materials and Methods (baseline subtraction, scaling, water vapor correction) with a quality control performed (described in Materials and Methods). Only spectra passing the quality controls were used to compute the means (**Figure 3A**). The PCA shown in **Figure 3B** reveals that the largest variance in samples from an individual donor is related to differences in lymphocyte subpopulations with the mean spectra largely clustering according to lymphocyte subset. PC1, which accounts for 60.7% of the total variance, separates B lymphocytes from T lymphocytes and PC2, which constitutes 18.9% of the total variance, separates  $CD4^+$  T lymphocytes from  $CD8^+$  T lymphocytes (**Figure 3C**). This data shows that lymphocytes have spectral differences over the entire IR region. A spectral normalization was performed principally on protein contributions present between  $1750$  and  $1480 \text{ cm}^{-1}$  (see Methods), the particular peaks in the  $3000$ - $2800 \text{ cm}^{-1}$  region of PC1 highlight a change in the lipid/protein ratio between T and B lymphocytes. Similar conclusions can be drawn for each donor (data not shown). These data show that in the absence of donor variability, B lymphocytes,  $CD4^+$  T lymphocytes and  $CD8^+$  T lymphocytes have distinct IR spectral characteristics.

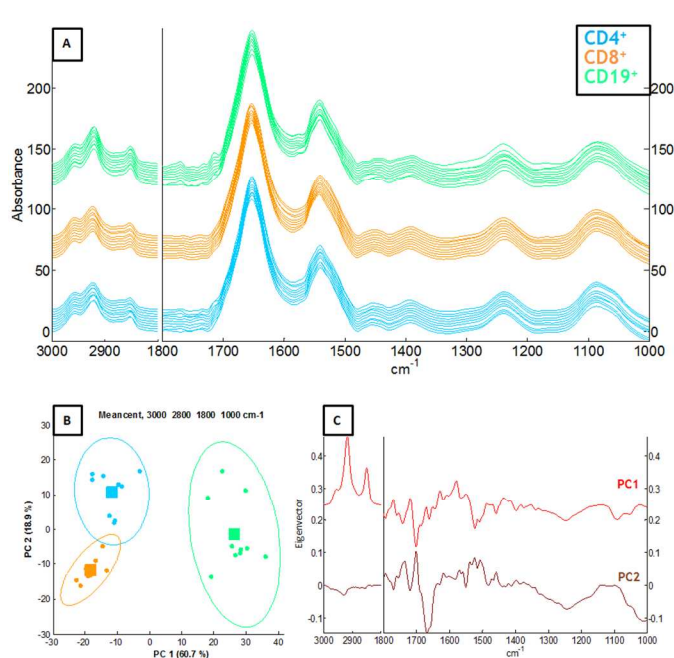


**Figure 3:** PCA of IR spectra recorded from the lymphocyte subpopulations isolated from one healthy donor. **A.** 28 mean spectra from purified unlabelled  $CD4^+$  T lymphocytes (blue),  $CD8^+$  T lymphocytes (orange) and  $CD19^+$  B lymphocytes (green) isolated from Donor 1's PB. Each spectrum is the mean of spectra obtained from one IR image. Spectra have been offset for visual clarity. **B.** Score plots showing the projection of each spectrum of Figure 3A in the PC1-PC2 space. The mean of each group is represented by a square surrounded by a 90 % confidence ellipse. The spectral range used for this analysis was the combined regions 3000-2800 and 1800-1000  $cm^{-1}$ . **C.** Principal components PC1 and PC2.

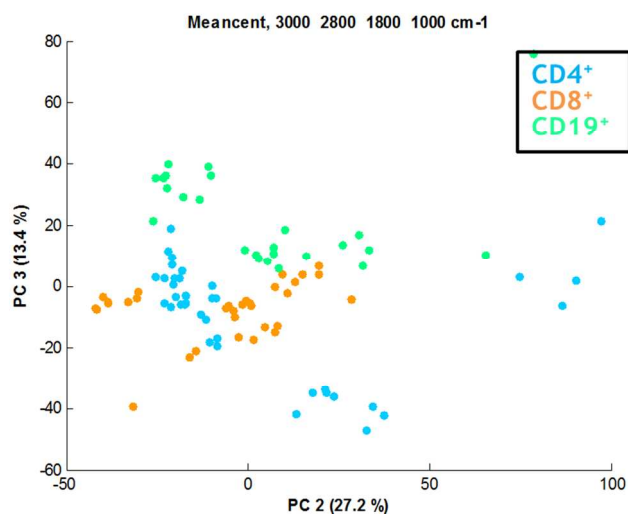


**Figure 4:** PCA of IR spectra recorded on lymphocyte subpopulations from different donors. Score plot showing the projection in the PC2-PC3 space of 99 mean spectra from purified  $CD4^+$  T lymphocytes (blue),  $CD8^+$  T lymphocytes (orange) and  $CD19^+$  B lymphocytes (green) isolated from all donors. The spectral range used for the analysis is the combined regions 3000-2800 and 1800-1000  $cm^{-1}$ .

When simultaneously analysing samples from different donors, the pattern is less clear. A PCA reveals that there is still a trend separating B from T lymphocytes based on PC2 and PC3 (**Figure 4**) but there is also separation related to the different donors (not illustrated). This could be anticipated because the various lymphocyte subpopulations have very similar spectra, and thus small variations between experiments could partially overwhelm the analysis. In turn, a supervised analysis could optimize lymphocyte subpopulation discrimination.

### Supervised statistical analyses

In the experiments described above we analysed mean IR spectra. However, if infrared imaging is going to be used for lymphocyte subpopulation identification, then it is also necessary for identification at pixel level. We therefore performed partial least square discriminant analyses (PLS-DA) to classify pixels, *i.e.* individual spectra, from different IR images of lymphocytes. First, a bootstrapping method (**Figure 5**) was used to produce an overview of the efficiency of the different spectral regions for lymphocyte subpopulation classification. In this analysis, spectral intervals were tested by restricted arbitrary blocks of 100  $cm^{-1}$ . 60% of the spectra were used to train a model with the remaining 40% used to test the model's quality. This procedure was repeated 40 times by randomly selecting a new training set and a new test set each time. A further check was performed to equilibrate the number of spectra in each class for both the training and test sets. The procedure was repeated for each spectral interval and a confusion matrix was obtained for each interval with a standard deviation. The most discriminant spectral regions are identifiable in **Figure 5**. The PCs (loadings) of the PCA performed on the mean IR spectra from each donor (**Figure 3**) indicate that spectral differences appear throughout the entire spectra of lymphocyte subpopulations. These data (**Figure 5**) clearly confirm that when considering individual spectra, *i.e.* individual pixels, most spectral regions contain information that discriminates between cellular subsets.

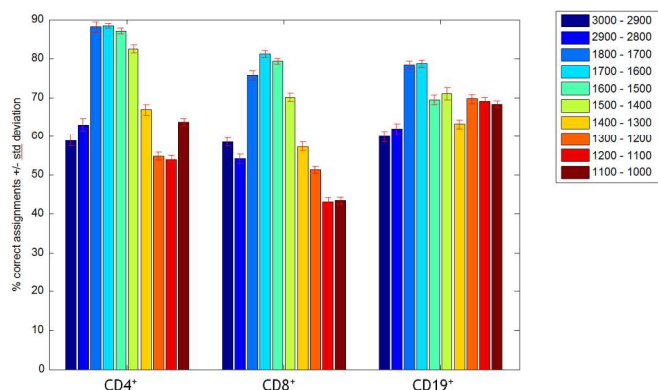


**Figure 5:** Interval PLS-DA performed on the individual IR spectra from lymphocytes. Success rate (in %) of the prediction models, as a function of the spectral range selected (see color legend). Interval PLS-DA classification was computed on a subset of 1500 randomly selected IR spectra from all donors (5000 IR spectra for each lymphocyte subpopulation). The percentages of correct assignment by the prediction models are reported on the Y axis; the predicted values are expressed as a percentage of the true values. The entire spectral range (3000-2800 and 1800-1000  $cm^{-1}$ ) was investigated by blocks of 100  $cm^{-1}$  (see color legend).

For all three lymphocyte subpopulations, the 1800-1400  $\text{cm}^{-1}$  spectral region is the most discriminant. Using only the 1700-1600  $\text{cm}^{-1}$  spectrum interval, a correct assignment score reaches 88, 82 and 78% for CD4<sup>+</sup>, CD8<sup>+</sup> and CD19<sup>+</sup> lymphocytes, respectively. When using the full spectral range (3000-2800 and 1800-1000  $\text{cm}^{-1}$ ), the correct assignment score reaches 91.8%, 87.6% and 87.7%, respectively (**Table 2**), which is significantly above the scores obtained for the best 100  $\text{cm}^{-1}$  interval alone. This indicates that other spectral regions contain non-redundant information useful for lymphocyte identification.

Recognition Model		Predicted as		
		CD4	CD8	CD19
True	CD4	90.8±0.7	7.9±0.6	1.4±0.3
	CD8	3.5±0.4	87.6±0.8	8.8±0.7
	CD19	2.0±0.3	10.4±0.7	87.7±0.7

**Table 2:** Lymphocyte subpopulation recognition model. Confusion matrix obtained by performing a supervised PLS-DA statistical analysis on a subset of 15,000 randomly selected IR spectra of lymphocytes recorded from each donor. The model was forced to take the same number of spectra in each group, i.e. 5,000 IR spectra for each lymphocyte subpopulation. 60% of the IR spectra recorded were used to train the model (training set) the remaining 40% were used to test the model (test set). Percentages in the matrix indicate the rate of correct assignment of the spectra to the lymphocyte subpopulation after 40 bootstrap iterations (mean ± standard deviation). The analysis was performed on the combined 3000-2800 and 1800-1000  $\text{cm}^{-1}$  spectral regions.

### Effect of the antibodies

This study was designed to isolate the major lymphocyte subpopulations without antibody labelling of the cells targeted for purification. Directly labelling the individual lymphocyte subpopulations with an antibody would make purification be more straightforward; however, potentially interfere with the spectral readings. Initially, it seemed unlikely that cell-bound antibody would significantly contribute to the infrared spectra. FTIR is sensitive to the mass of material present in the beam and the weight of bound antibody would be negligible with respect to the weight of total cellular proteins. The data shown in **Figure 6** nevertheless show there are significant differences in each lymphocyte subpopulation isolated with or without antibody labelling. Examination of the PCs (not shown) did not detect any significant changes in the amide I – amide II range. In particular, the spectral features typical of the  $\beta$ -sheet structure of an antibody were not observed but changes were present throughout the spectrum suggesting that antibody binding triggered a cellular response that modified their metabolism. This observation underscores the importance of taking infrared spectra from lymphocytes that have been minimally manipulated.

### Discussion

The data presented in this study demonstrate the usefulness of FTIR imaging to phenotype PB lymphocytes. In preparation for IR recording, we designed a flow cytometric sorting procedure for isolating unlabelled lymphocytes from healthy donor PB, i.e. negative purification. This approach has the advantage of harvesting a specific lymphocyte subpopulation with a high degree of purity without antibody bound to the cell surface.

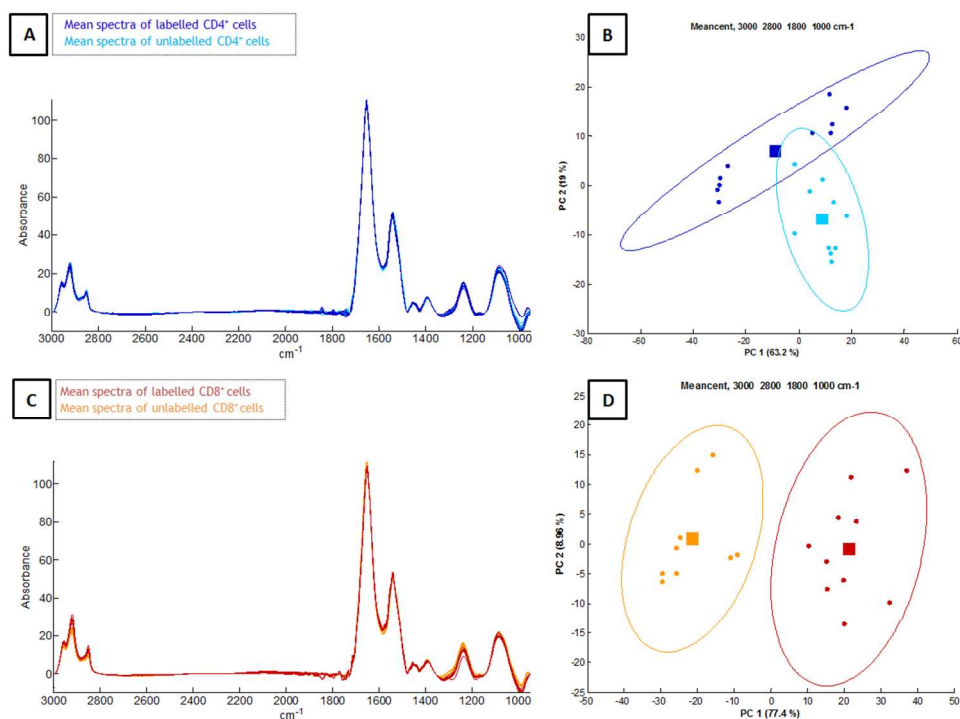


**Figure 6:** PCA of IR spectra recorded on labelled lymphocytes and unlabelled lymphocytes from one donor. **A.** Ten IR spectra from CD4<sup>+</sup> T cells labelled with antibodies (dark blue) and ten IR spectra from unlabelled CD4<sup>+</sup> T cells (light blue) isolated from the peripheral blood of Donor 1. Each spectrum is the mean of spectra obtained on one IR image (details in Materials and Methods). CD4<sup>+</sup> labelled cells were isolated by flow cytometry using a human anti-CD4 FITC-conjugated antibody. Unlabelled CD4 cells were obtained by negative cell isolation. **B.** Score plots showing the projection of each spectrum from Figure 6A in the PC1-PC2 space. The percentage of variance explained by each PC appears on the axes. The mean of each group is represented by a square surrounded by a 90 % confidence ellipse. The spectral range used for this analysis are the combined 3000-2800 and 1800-1000  $\text{cm}^{-1}$  regions. **C.** and **D.** The same as A and B for CD8<sup>+</sup> T cells labelled with anti-CD8 antibody (red) and unlabelled (orange).

1 This negative sorting procedure circumvents spectral  
2 contributions by the fluorophore-conjugated antibody, which  
3 we found were detectable, as well as potential metabolic  
4 triggering of cellular pathways by antibody binding that can  
5 influence lymphocyte IR spectra. This approach could be  
6 effectively used for other experiments to select specific  
7 lymphocyte subpopulations, such as subsets of CD4<sup>+</sup> T or  
8 CD19<sup>+</sup> B lymphocytes, without an antibody presence on the  
9 target population. The influence of antibody binding on IR  
10 spectra demonstrated emphasizes their sensitivity to any  
11 environmental change. It is also likely that IR spectra taken  
12 from sorted PB lymphocytes will also be different from the  
13 spectra obtained from tissue sections due both to differences in  
14 sample processing<sup>16</sup> and the *in vivo* microenvironment from  
15 which they were isolated.

16 Lymphocyte subpopulations could be easily distinguished  
17 by unsupervised statistical analyses for each healthy donor but  
18 inter-donor variability required the use of supervised  
19 approaches to separate lymphocyte subpopulations at image  
20 pixel level. Results are encouraging showing a correct  
21 discrimination rate of 87 to 91% for the three lymphocyte  
22 subpopulations, *i.e.* in the range of the purity achieved by cell  
23 sorting. This suggests that a common spectral signature exists  
24 between the different donors suggesting it has potential for  
25 imaging. The data presented here also confirm the ability of  
26 FTIR imaging to distinguish between T and B lymphocytes,  
27 which was first shown by Krafft et al.<sup>59</sup> In this study, we  
28 further demonstrate that FTIR imaging can effectively  
29 discriminate unlabelled CD4<sup>+</sup> helper T lymphocytes cells from  
30 CD8<sup>+</sup> cytotoxic T lymphocytes cells, two T cell subpopulations  
31 derived from a common ancestral cell that differentiate to serve  
32 specific functions in the adaptive immune response. The work  
33 presented here provides a foundation for future studies of  
34 lymphocyte metabolism and differentiation by IR imaging.  
35 Distinguishing between naive and memory T or B  
36 lymphocytes, activated and resting lymphocytes<sup>57,58</sup> or the  
37 myriad of helper CD4<sup>+</sup> T lymphocytes (Th1, Th2, Th17, Tfh  
38 and regulatory T lymphocytes) based on their IR spectral  
39 features are examples of studies in progress or for exploration  
40 in the near future.

41 The data reported here were obtained with a particular  
42 processing that includes rather arbitrary selection of baseline  
43 and normalization, which could potentially influence the results  
44 of the analysis. Amide bands are major contributors to  
45 discrimination and are prone to include resonant Mie scattering  
46 contributions. In turn, normalizing on amide bands could lead  
47 to true discrimination but largely based on Mie scattering  
48 effects, related more to the physical morphology of the cells  
49 and less on differences in their chemical composition. Pre-  
50 processing has been a matter of concern for years and there is  
51 still no consensus on a solution.<sup>67</sup> Previously, we evaluated the  
52 effects of various pre-processing approaches on the  
53 discriminatory power of FTIR spectroscopy with series of  
54 ATR-FTIR spectra containing typical perturbations (baseline  
55 shift, scaling factor, and noise)<sup>68</sup>. Both synthetic spectra and  
56 cell spectra were analysed. Several baseline-correction and  
57 normalization possibilities were evaluated. Our results were  
58 generally sensitive, selective, and robust with respect to  
59 baseline and scaling. Vector normalization did not improve  
60 discrimination and derivative spectra were not more efficient,  
but were less sensitive to scaling. To address this further, in  
this study second derivative spectra were obtained after  
correction for water vapor and CO<sub>2</sub> (described in Materials and  
Methods), full vector normalization was performed on the

3000-2800 and 1586-1000 cm<sup>-1</sup> combined spectral regions *i.e.*  
without considering the Amide I region. This pre-processing  
method is expected to minimize potential resonant Mie  
scattering artefacts, which are usually large in the Amide I  
spectral range, and avoid normalization on the Amide bands  
only. Principle component analysis (**Figure S1**) revealed that  
the separation achieved between cell types is very similar to the  
data presented in **Figure 3**. This strongly suggests that the  
separation shown in **Figure 3** is principally based on variation  
in the biochemical composition of these cells.

Discrimination and identification of lymphocyte  
subpopulations on tissue sections using FTIR imaging remains  
a controversial subject, essentially because of the lack of a  
solid histochemical reference for each spectrum of the FTIR  
image. The work reported in this study lays a foundation for  
future studies on histological sections since lymphocytes are  
frequently present either as isolated cells or aggregates in  
tissues. Identifying lymphocyte subpopulations with precision  
will require a complex set of experiments where, after IR  
imaging, the various lymphocyte subpopulations are  
simultaneously recognized on the same tissue section. While  
our results show that FTIR imaging is able to discriminate  
between PB lymphocyte subpopulations, the clinical utility of  
this vibrational technique remains to be demonstrated. For  
example, its ability to discriminate between different  
lymphocyte subpopulations infiltrating a solid tumor has yet to  
be achieved because tissue sections are very complex  
structures. The particular microenvironment present in a tumor  
could influence the lymphocyte IR spectra due to biochemical  
influences by tumor cells, stromal cells, endothelial cells, the  
extracellular matrix, etc., which are in contact with the  
infiltrated lymphocytes. Additionally, there may be spectral  
contributions by the surrounding tissue to the lymphocyte IR  
spectra that could affect classification accuracy. Nevertheless,  
some published studies suggest lymphocytes can be recognized  
on tissue sections.<sup>58,59</sup> Furthermore, to maximize accurate  
lymphocyte identification and cell subpopulation  
discrimination on tissue sections using IR imaging, we believe  
it is important to use reference spectra recorded on identically  
pre-processed tissue samples.

The impact of cell-bound antibodies shown here is likely  
related to cellular activities triggered by antibody binding to  
live cells and not the antibodies themselves. IR spectroscopy  
contributions depend on the weight of the different molecules  
present in the beam and antibodies bound to a specific receptor  
on the lymphocyte surface likely represent a small fraction of  
the proteins present in the IR beam. On the other hand, some of  
these receptors function to trigger cellular pathways whose  
activities could significantly influence the IR spectra. The  
effect of antibody binding to fixed cells in tissue sections is  
expected to be insignificant.

In conclusion, this study has shown that FTIR imaging is a  
reliable tool for discriminating between the major lymphocyte  
subpopulations in the absence of antibody labelling or  
histochemical staining. This vibrational technique promises to  
be a useful tool for discriminating and potentially identifying  
the subpopulation specificity of tumor infiltrating lymphocytes,  
an important prognostic and predictive factor in the  
management of breast cancer.<sup>46-50</sup>

## Acknowledgments

The authors would like to express their sincere gratitude to the donors who contributed to this study. This research has been supported by grants from the National Fund for Scientific Research (FRFC 2.4526.12, 2.4527.10 and T.0155.13). E.G. is Research Director with the National Fund for Scientific Research (FNRS) (Belgium), M.V. is Research Fellow supported by the Fund for Research and Education within Industry and Agriculture (FRIA) from the FNRS (Belgium).

## Notes

<sup>a</sup> Laboratory for the Structure and Function of Biological Membranes, Center for Structural Biology and Bioinformatics, Université Libre de Bruxelles, Campus Plaine, Bd du Triomphe 2, CP206/02, B1050 Brussels, Belgium. *E-mail*: egor@ulb.ac.be; Fax: +32 2 650 53 82; Tel: +32 2 650 53 86.

<sup>b</sup> Molecular Immunology Unit, Institut Jules Bordet, Université Libre de Bruxelles, Brussels, Belgium ;

<sup>c</sup> Flow Cytometry Unit, Institut Jules Bordet, Université Libre de Bruxelles, Brussels, Belgium.

## Abbreviations

APC, Allophycocyanin; CD, Cluster of Differentiation; EDTA, Ethylenediaminetetraacetic acid; FACS, Fluorescence Activated Cell Sorter/ing; FITC, Fluorescein Isothiocyanate Conjugate; FPA, Focal Plane Array; FTIR, Fourier Transform Infrared; HD, Healthy Donors; IF, Immunofluorescence; IHC, Immunohistochemical; IR, Infrared; LT, Lymphocyte T; LB, Lymphocyte B; MCT, Mercury Cadmium Telluride; PB, Peripheral Blood; PBMC, Peripheral Blood Mononuclear Cell; PCA, Principal Component Analysis; PC, Principal Component; PE, Phycoerythrin; PLS-DA, Partial Least Square Discriminant Analysis; rpm, rounds per minute; RPMI: Roswell Park Memorial Institute (cell culture medium); S/N, Signal to Noise; TIL, Tumor Infiltrating Lymphocyte.

## References

1. E. Kleiren, J. M. Ruyschaert, E. Goormaghtigh, and V. Raussens, *Spectrosc. Int. J.*, 2010, **24**, 61–66.
2. H. H. de Jongh, E. Goormaghtigh, and J. M. Ruyschaert, *Biochemistry*, 1997, **36**, 13603–13610.
3. E. Goormaghtigh, V. Cabiliaux, and J. M. Ruyschaert, *Subcell. Biochem.*, 1994, **23**, 405–450.
4. E. Goormaghtigh, R. Gasper, A. Benard, A. Goldsztein, and V. Raussens, *Biochim Biophys. Acta-Proteins Proteomics*, 2009, **1794**, 1332–1343.
5. E. Goormaghtigh, J. M. Ruyschaert, and V. Raussens, *Biophys. J.*, 2006, **90**, 2946–2957.
6. A. Derenne, T. Claessens, C. Conus, and E. Goormaghtigh, in *Encyclopedia of Biophysics*, 2013, pp. 1074–1081.
7. A. Derenne, O. Vandersleyen, and E. Goormaghtigh, *Biochim. Biophys. Acta*, 2013.
8. S. Boydston-White, T. Gopen, S. Houser, J. Bargonetti, and M. Diem, *Biospectroscopy*, 1999, **5**, 219–27.
9. H. N. Holman, M. C. Martin, E. A. Blakely, K. Bjornstad, and W. R. McKinney, *Biopolymers*, 2000, **57**, 329–335.
10. S. Boydston-White, T. Chernenko, A. Regina, M. Miljkovic, C. Matthaus, and M. Diem, *Vib. Spectrosc.*, 2005, **38**, 169–177.

11. S. Boydston-White, M. Romeo, T. Chernenko, A. Regina, M. Miljkovic, and M. Diem, *Biochim. Biophys. Acta-Biomembranes*, 2006, **1758**, 908–914.
12. K. R. Flower, I. Khalifa, P. Bassan, D. Démoulin, E. Jackson, N. P. Lockyer, A. T. McGown, P. Miles, L. Vaccari, and P. Gardner, *Analyst*, 2011, **136**, 498–507.
13. C. Hughes, M. D. Brown, F. J. Ball, G. Monjardez, N. W. Clarke, K. R. Flower, and P. Gardner, *Analyst*, 2012, **137**, 5736–42.
14. A. Derenne, A. Mignolet, and E. Goormaghtigh, *Analyst*, 2013, **138**, 3998–4005.
15. R. Gasper and E. Goormaghtigh, *Analyst*, 2010, 3048–3051.
16. M. Verdonck, N. Wald, J. Janssis, P. Yan, C. Meyer, A. Legat, D. E. Speiser, C. Desmedt, D. Larsimont, C. Sotiriou, and E. Goormaghtigh, *Analyst*, 2013, **138**, 4083–91.
17. A. Derenne, R. Gasper, and E. Goormaghtigh, *Analyst*, 2011, **136**, 1134–1141.
18. R. Gasper, T. Mijatovic, A. Bénard, A. Derenne, R. Kiss, and E. Goormaghtigh, *Biochim. Biophys. Acta*, 2010, **1802**, 1087–94.
19. A. Derenne, M. Verdonck, and E. Goormaghtigh, *Analyst*, 2012, **137**, 3255–64.
20. R. Gasper, J. Dewelle, R. Kiss, T. Mijatovic, and E. Goormaghtigh, *Biochim. Biophys. Acta*, 2009, **1788**, 1263–70.
21. R. Gasper, T. Mijatovic, R. Kiss, and E. Goormaghtigh, *Appl. Spectrosc.*, 2011, **65**, 584–594.
22. R. Gasper, G. Vandebussche, and E. Goormaghtigh, *Biochim. Biophys. Acta*, 2011, **1808**, 597–605.
23. R. Bhargava, *Anal. Bioanal. Chem.*, 2007, **389**, 1155–69.
24. G. Bellisola and C. Sorio, *Am. J. Cancer Res.*, 2012, **2**, 1–21.
25. P. Lasch, L. Chiriboga, H. Yee, and M. Diem, *Technol. Cancer Res. Treat.*, 2002, **1**, 1–7.
26. P. Lasch, M. Diem, W. Hänsch, and D. Naumann, *J. Chemom.*, 2007, **20**, 209–220.
27. M. J. Walsh, M. J. German, M. Singh, H. M. Pollock, A. Hammiche, M. Kyrgiou, H. F. Stringfellow, E. Paraskevaidis, P. L. Martin-Hirsch, and F. L. Martin, *Cancer Lett.*, 2007, **246**, 1–11.
28. G. J. Ooi, J. Fox, K. Siu, R. Lewis, K. R. Bamberg, D. McNaughton, and B. R. Wood, *Med. Phys.*, 2008, **35**, 2151–61.
29. B. Bird, M. Romeo, N. Laver, and M. Diem, *J. Biophotonics*, 2009, **2**, 37–46.
30. M. J. Walsh, A. Kajdacsy-Balla, S. E. Holton, and R. Bhargava, *Vib. Spectrosc.*, 2012, **60**, 23–28.
31. A. Bénard, C. Desmedt, M. Smolina, P. Szternfeld, M. Verdonck, G. Rouas, N. Kheddoumi, F. Rothé, D. Larsimont, C. Sotiriou, and E. Goormaghtigh, *Analyst*, 2014, **139**, 1044–56.
32. M. J. German, A. Hammiche, N. Ragavan, M. J. Tobin, L. J. Cooper, S. S. Matanhelia, A. C. Hindley, C. M. Nicholson, N. J. Fullwood, H. M. Pollock, and F. L. Martin, *Biophys. J.*, 2006, **90**, 3783–95.
33. E. Gazi, M. Baker, J. Dwyer, N. P. Lockyer, P. Gardner, J. H. Shanks, R. S. Reeve, C. A. Hart, N. W. Clarke, and M. D. Brown, *Eur. Urol.*, 2006, **50**, 750–60; discussion 760–1.
34. M. J. Baker, E. Gazi, M. D. Brown, J. H. Shanks, P. Gardner, and N. W. Clarke, *Br. J. Cancer*, 2008, **99**, 1859–66.
35. M. J. Baker, E. Gazi, M. D. Brown, J. H. Shanks, N. W. Clarke, and P. Gardner, *J. Biophotonics*, 2009, **2**, 104–13.
36. P. D. Lewis, K. E. Lewis, R. Ghosal, S. Bayliss, A. J. Lloyd, J. Wills, R. Godfrey, P. Kloer, and L. A. J. Mur, *BMC Cancer*, 2010, **10**, 640.
37. B. Bird, M. S. Miljković, S. Remiszewski, A. Akalin, M. Kon, and M. Diem, *Lab. Invest.*, 2012, **92**, 1358–73.
38. P. Lasch, W. Haensch, D. Naumann, and M. Diem, *Biochim. Biophys. Acta*, 2004, **1688**, 176–86.
39. A. Travo, O. Piot, R. Wolthuis, C. Gobinet, M. Manfait, J. Bara, M.-E. Forgue-Lafitte, and P. Jeannesson, *Histopathology*, 2010, **56**, 921–31.
40. A. Kallenbach-Thieltges, F. Großerüschkamp, A. Mosig, M. Diem, A. Tannapfel, and K. Gerwert, *J. Biophotonics*, 2013, **6**, 88–100.
41. J. Nallala, O. Piot, M.-D. Diebold, C. Gobinet, O. Bouché, M. Manfait, and G. D. Sockalingum, *Cytometry. A*, 2013, **83**, 294–300.
42. P. T. Wong, S. M. Goldstein, R. C. Grekin, T. A. Godwin, C. Pivik, and B. Rigas, *Cancer Res.*, 1993, **53**, 762–5.

- 1 43. F. Le Naour, M.-P. Bralet, D. Debois, C. Sandt, C. Guettier, P. Dumas,  
2 A. Brunelle, and O. Lapr evote, *PLoS One*, 2009, **4**, e7408.
- 3 44. L. Quaroni and A. G. Casson, *Analyst*, 2009, **134**, 1240–6.
- 4 45. N. Bergner, B. F. M. Romeike, R. Reichart, R. Kalf , C. Krafft, and J.  
5 Popp, *Analyst*, 2013, **138**, 3983–90.
- 6 46. F. Pag s, J. Galon, M.-C. Dieu-Nosjean, E. Tartour, C. Saut s-Fridman,  
7 and W.-H. Fridman, *Oncogene*, 2010, **29**, 1093–102.
- 8 47. W. H. Fridman, J. Galon, F. Pag s, E. Tartour, C. Saut s-Fridman, and  
9 G. Kroemer, *Cancer Res.*, 2011, **71**, 5601–5.
- 10 48. J. Galon, F. Pag s, F. M. Marincola, M. Thurin, G. Trinchieri, B. A.  
11 Fox, T. F. Gajewski, and P. A. Ascierto, *J. Transl. Med.*, 2012, **10**, 1.
- 12 49. C. Gu-Trantien, S. Loi, S. Garaud, C. Equeter, M. Libin, A. de Wind, M.  
13 Ravoet, H. Le Buanec, C. Sibille, G. Manfouo-Foutsop, I. Veys, B.  
14 Haibe-Kains, S. K. Singhal, S. Michiels, F. Roth , R. Salgado, H.  
15 Duvillier, M. Ignatiadis, C. Desmedt, D. Bron, D. Larsimont, M. Piccart,  
16 C. Sotiriou, and K. Willard-Gallo, *J. Clin. Invest.*, 2013, **123**, 2873–92.
- 17 50. R. Salgado, C. Denkert, S. Demaria, N. Sirtaine, F. Klauschen, G.  
18 Pruneri, S. Wienert, G. Van den Eynden, F. L. Baehner, F. Penault-  
19 Llorca, E. A. Perez, E. A. Thompson, W. F. Symmans, A. L.  
20 Richardson, J. Brock, C. Criscitiello, H. Bailey, M. Ignatiadis, G. Floris,  
21 J. Sparano, Z. Kos, T. Nielsen, D. L. Rimm, K. H. Allison, J. S. Reis-  
22 Filho, S. Loibl, C. Sotiriou, G. Viale, S. Badve, S. Adams, K. Willard-  
23 Gallo, and S. Loi, *Ann. Oncol.*, 2014, *in press*.
- 24 51. C. Gu-Trantien and K. Willard-Gallo, *Oncoimmunology*, 2013, **2**,  
25 e26066.
- 26 52. C. Denkert, S. Loibl, A. Noske, M. Roller, B. M. M ller, M. Komor, J.  
27 Budczies, S. Darb-Esfahani, R. Kronenwett, C. Hanusch, C. von T rme,  
28 W. Weichert, K. Engels, C. Solbach, I. Schrader, M. Dietel, and G. von  
29 Minckwitz, *J. Clin. Oncol.*, 2010, **28**, 105–13.
- 30 53. C. P. Schultz, K. Liu, J. B. Johnston, and H. H. Mantsch, *Leuk. Res.*,  
31 1996, **20**, 649–655.
- 32 54. C. P. Schultz, K.-Z. Liu, J. B. Johnston, and H. H. Mantsch, *J. Mol.*  
33 *Struct.*, 1997, **408-409**, 253–256.
- 34 55. S. Mordechai, J. Ramesh, C. Levi, M. Huleihal, V.  
35 Erukhimovitch, A. Moser, and J. Kapelushnik, in *International*  
36 *Symposium on Optical Science and Technology*, ed. C. Nguyen,  
37 International Society for Optics and Photonics, 2001, pp. 243–250.
- 38 56. N. Gault and J.-L. Lefaix, *Radiat. Res.*, 2003, **160**, 238–50.
- 39 57. B. R. Wood, B. Tait, and D. McNaughton, *Hum. Immunol.*, 2000, **61**,  
40 1307–1314.
- 41 58. A. I. Mazur, J. L. Monahan, M. Miljkovi , N. Laver, M. Diem, and B.  
42 Bird, *J. Biophotonics*, 2013, **6**, 101–9.
- 43 59. C. Krafft, R. Salzer, G. Soff, and M. Meyer-Hermann, *Cytometry. A*,  
44 2005, **64**, 53–61.
- 45 60. E. Goormaghtigh and J.-M. Ruyschaert, *Spectrochim. Acta*, 1994, **50**,  
46 2137–2144.
- 47 61. E. Goormaghtigh, in *Adv. Biomed. Spectrosc.*, vol. 2, eds. A. Barth and  
48 P. I. Haris, 2009, pp. 104–128.
- 49 62. P. Bassan, A. Kohler, H. Martens, J. Lee, E. Jackson, N. Lockyer, P.  
50 Dumas, M. Brown, N. Clarke, and P. Gardner, *J. Biophotonics*, 2010, **3**,  
51 609–20.
- 52 63. P. Bassan, A. Sachdeva, A. Kohler, C. Hughes, A. Henderson, J. Boyle,  
53 J. H. Shanks, M. Brown, N. W. Clarke, and P. Gardner, *Analyst*, 2012,  
54 **137**, 1370–7.
- 55 64. B. Bird, M. Miljkovi , and M. Diem, *J. Biophotonics*, 2010, **3**, 597–608.
- 56 65. K. R. Bambery, B. R. Wood, and D. McNaughton, *Analyst*, 2012, **137**,  
57 126–32.
- 58 66. A. Dazzi, A. Deniset-Besseau, and P. Lasch, *Analyst*, 2013, **138**, 4191–  
59 201.
- 60 67. M. J. Baker, J. Trevisan, P. Bassan, R. Bhargava, H. J. Butler, K. M.  
Dorling, P. R. Fielden, S. W. Fogarty, N. J. Fullwood, K. A. Heys, C.  
Hughes, P. Lasch, P. L. Martin-Hirsch, B. Obinaju, G. D. Sockalingum,  
J. Sul -Suso, R. J. Strong, M. J. Walsh, B. R. Wood, P. Gardner, and F.  
L. Martin, *Nat. Protoc.*, 2014, **9**, 1771–91.
68. A. Gaigneaux, J. M. Ruyschaert, and E. Goormaghtigh, *Appl.*  
*Spectrosc.*, 2006, **60**, 1022–1028.

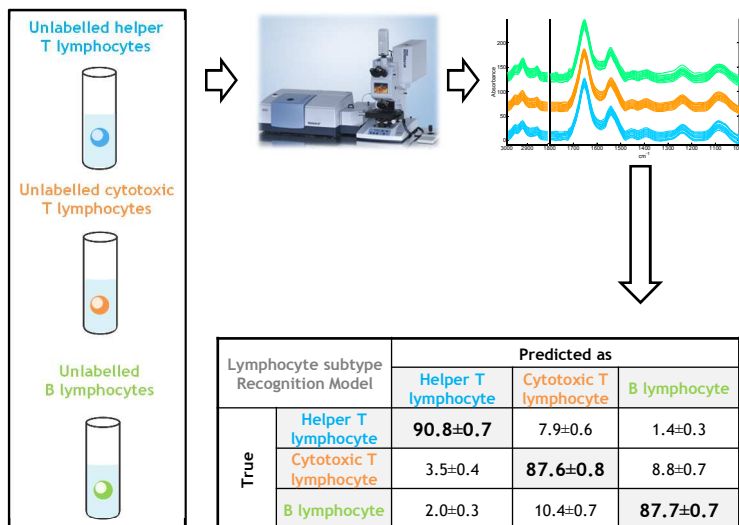
Journal Name

RSCPublishing

ARTICLE

Analyst Accepted Manuscript

FTIR imaging enables to effectively discriminate lymphocyte subpopulations without antibody labelling



1  
2  
3  
4  
5  
6  
7  
8  
9  
10  
11  
12  
13  
14  
15  
16  
17  
18  
19  
20  
21  
22  
23  
24  
25  
26  
27  
28  
29  
30  
31  
32  
33  
34  
35  
36  
37  
38  
39  
40  
41  
42  
43  
44  
45  
46  
47  
48  
49  
50  
51  
52  
53  
54  
55  
56  
57  
58  
59  
60